

# Particle multiplicities at LHC and deviations from limiting fragmentation

**Jianhong Ruan and Wei Zhu**

Department of Physics, East China Normal University, Shanghai 200062, P.R. China

## **Abstract**

The pseudorapidity density of charged particles produced at LHC collisions are predicted by using two complementary production mechanisms with a set of consistent integrated and unintegrated parton distributions. We discuss the limiting fragmentation hypothesis and its possible violation, and we compare our model with other partonic models.

PACS number(s): 12.38.Bx, 13.60.Hb, 24.85.+p, 25.75.-q

# 1 Introduction

Particle multiplicity distribution is one of the first measurements to be taken at the CERN Large Hadron Collider (LHC). The upcoming data on its energy, centrality, and rapidity dependence are expected to discriminate various (integrated and unintegrated) parton distributions, which are basic quantities analyzing high-energy reactions on the parton level. The Bjorken variable  $x$  of gluons may reach very small values at LHC energies. Therefore, the nonlinear corrections of the initial gluon correlations to the QCD evolution equations should be considered in any available parton distributions of the LHC physics [1].

One of the striking predictions of nonlinear QCD evolution equations is the saturation solution of the Jalilian-Marian-Iancu-McLerran-Weigert-Leonidov-Kovner (JIMWLK) equation [2], where the unintegrated gluon distribution is absolutely flat in  $k_t$ -space at  $k_t < Q_s$ ;  $Q_s$  is the saturation scale and the relating phenomenon is called the color glass condensate (CGC). The above saturation solution was proved in the numerical solutions of the JIMWLK equation [3]. Instead of the complicated JIMWLK equation, which is equivalent to an infinite, coupled hierarchy of evolution equations (the Balitsky hierarchies), much of the physics content has been studied with the help of approximations, such as the Balitsky-Kovchegov (BK) equation [4], or outright models that capture the main features as they affect specific phenomena, such as the Kharzeev-Levin (KL) model [5] does for the present context.

The KL model mimics a possible saturation solution of the JIMWLK equation, and it assumes that the scale  $Q_s^2(x) \equiv Q_0^2(x_0/x)^\lambda$ . Under some additional assumptions, Kharzeev, Levin, and Nardi (KLN) use this model successfully to explain some of the climactical data

probed at the BNL Relativistic Heavy-Ion Collider (RHIC) and to predict LHC physics [6]. The BK equation is regarded as the leading order approximation of the JIMWLK equation and preserves the saturation and scaling features. Albacete uses the BK equation to predict the pseudorapidity density of charged particles produced in central  $Pb - Pb$  collisions at LHC [7].

However, both the KL model and BK equation work at a very small  $x$  range, (for say,  $x < x_0$ ,  $x_0 \ll 10^{-1}$ ), where the saturation begins work. The  $x$ -dependence of the gluon density at  $x > x_0$  in these works [6,7] are simply fixed to be  $(1-x)^4$ , which is un-evolution. As we have pointed out, the parton distributions at intermediate and larger  $x$  influence the shape of the rapidity spectrum [8]. In fact, Szczurek uses the same KL model but with different factors  $\sim (1-x)^{5-7}$  and obtains a narrower pseudo-rapidity distribution [9]. Anyway, a fixed form  $\sim (1-x)^4$  for an available gluon distribution is too rough. Obviously, as a complement to the above-mentioned saturation models, it is necessary to consider the parton distributions, which are well defined in a broad kinematic range.

Besides, some works [6,7] have used a single production mechanism, i.e., gluon-gluon fusion  $gg \rightarrow g$ , which is proposed by Gribov, Levin and Ryskin (GLR) [10] to predict particle production. However, the single-particle inclusive spectrum shows that its rapidity distribution has three distinct regions: a central region with two (project and target) fragmentation regions [11]. The GLR model is expected to dominate the processes at the central region. Therefore, other collision dynamics in the fragmentation regions should be considered. There are several two-component models for hadron collisions. For example, the HIJING model [12] is such a two-component model. This model uses the parameterized integrated parton distributions to compute multiple minijet production and incor-

porates the Lund string model [13] to model soft beam jet fragmentation. However, the production of minijets at the central region should be described by the unintegrated gluon distribution rather than the integrated gluon density [9]. Moreover, the string model is irrelevant to the parton distributions. In the same model, the hard and soft components based on different basic physical parameters may lose some interesting information about heavy-ion collisions.

In this work, we use a two-component model and a set of consistent parton distributions to improve the above-mentioned situation of the present models. Basically, we use two complementary production mechanisms: the hard gluon-gluon fusion [10] and the soft quark recombination [14]. Our picture is as follows. At sufficiently high-energy hadron-hadron collisions, particles produced in hard gluon-gluon fusions are distributed in a region around midrapidity, and these initial gluons are described by the unintegrated gluon distribution in both colliding hadrons. On the other hand, the valence quarks tend to fly through with their original integrated distributions and they are hadronized by recombining with additional low- $x$  sea quarks from the central region. The resulting soft recombined particles dominate the fragmentation region. We shall present the related formula of two production mechanisms in Sec.II. Because gluon fusion and quark recombination use unintegrated and integrated parton distributions, respectively, a set of these parton distributions, which are defined in a broad kinematic range are necessary. In our previous work [8], we proposed such distributions in protons and heavy nuclei by using a modified Dokshitzer-Gribov- Lipatov-Altarelli-Parisi (MD-DGLAP) equation [15], which incorporates the shadowing and antishadowing corrections. Unlike the JIMWLK and BK equations, MD-DGLAP equation works in a broad pre-saturation range. We shall

use these parton distributions to explain the particle multiplicity distributions in UA5 and RHIC data, then we will predict the particle multiplicity distributions at LHC in Secs. III and IV. Unfortunately, we can not theoretically predict the energy dependence of the normalization of the hadronic distributions, which is fixed using the entirely phenomenological parametrization of existing data in this work. This simple method may need modification after we obtain the LHC data at midrapidity.

In Sec. V we discuss some interesting properties of rapidity distributions. Limiting fragmentation [16] and rapidity plateau [17] are characteristics of two components of particle production. We find that the limiting fragmentation hypothesis, which generally appears in present data of hadron collisions is partly violated if the observations are over a wide range between the RHIC and LHC energies. An explanation of limiting fragmentation and its violation in partonic picture is given. On the other hand, we propose that a possible quark gluon plasma (QGP) effect may deform the shape of the central plateau. We also discuss the nuclear shadowing effects in heavy-ion collisions. The comparisons of our predictions with those of saturation models are given in this section. The above-mentioned properties of particle multiplicity distributions in the partonic models of hadron collisions, except for their height at midrapidity, are dominated by the parton distributions. Therefore, the results potentially tell us how parton distributions evolve at high energies. The last section is a short summary of this study.

## 2 Two-component model

The single-particle inclusive spectrum shows a rapidity distribution with three distinct regions: a central region and two (project and target) fragmentation regions. We assume that the hadrons produced in the central region (small  $x$  and large  $k_t$ ) are produced from the hadronization of the gluons in the  $gg \rightarrow g$  mechanism [10], while the particles in the fragmentation region are formed by the valence quarks according to the quark recombination model [14]. The related formulas are summarized as follows.

Component I. The cross section for inclusive gluon production in  $pp \rightarrow g$  through the gluonic mechanism  $gg \rightarrow g$  at sufficiently high energy reads [10]

$$\begin{aligned} & \frac{d\sigma_{p-p}^I(y, p_{t,g})}{dy d^2 p_{t,g}} \\ &= \frac{4N_c}{N_c^2 - 1} \frac{1}{p_{t,g}^2} \int d^2 q_{t,g} \alpha_s(\Omega) F_g^p \left( x_1, \left( \frac{p_{t,g} + q_{t,g}}{2} \right)^2, p_{t,g}^2 \right) F_g^p \left( x_2, \left( \frac{p_{t,g} - q_{t,g}}{2} \right)^2, p_{t,g}^2 \right), \end{aligned} \quad (1)$$

where  $\Omega = \max(k_{1t}^2, k_{2t}^2, p_{t,g}^2)$ ,  $k_{1,t}^2 = \frac{1}{4}(p_{t,g} + q_{t,g})^2$  and  $k_{2,t}^2 = \frac{1}{4}(p_{t,g} - q_{t,g})^2$ ; The rapidity  $y$  of the produced gluon in the center-of-mass frame of  $p - p$  collisions is defined by

$$x_{1/2} = \frac{p_{t,g}}{\sqrt{s}} \cdot \exp(\pm y); \quad (2)$$

$F_g^p(x, k_t^2, p_t^2)$  is the two scale unintegrated gluon distribution in the proton. A general relation between integrated and unintegrated parton distributions is

$$\int_0^{\mu^2} dk_t^2 F_a^p(x, k_t^2, \mu^2) = x a_p(x, \mu^2), \quad (3)$$

where  $a_p(x, \mu^2) = v_p(x, \mu^2)$ ,  $s_p(x, \mu^2)$  and  $g_p(x, \mu^2)$  imply the integrated valence quark, sea quark and gluon distributions in the proton.

In experiments a good identification of particles is to measure pseudorapidity. The relation between the rapidity  $y$  and pseudorapidity  $\eta$  for massive particles is

$$y = \frac{1}{2} \ln \left[ \frac{\sqrt{\frac{m_{eff}^2 + p_t^2}{p_t^2} + \sinh^2 \eta} + \sinh \eta}{\sqrt{\frac{m_{eff}^2 + p_t^2}{p_t^2} + \sinh^2 \eta} - \sinh \eta} \right], \quad (4)$$

where  $m_{eff}$  is the typical invariant mass of the gluon mini-jet.

For avoiding the complicate hadronization dynamics, similar to Ref. [9], we use local parton-hadron duality, i.e., the rapidity distribution of particles is identical to the rapidity distribution of gluons:  $\eta_g = \eta_h \equiv \eta$ . Thus, the pseudorapidity density of produced charged particles in  $p - p$  collisions is given by

$$\begin{aligned} & \frac{dN_{p-p}^I}{d\eta} \\ &= \frac{1}{\sigma_{in}} \int d^2 p_{t,h} \frac{d\sigma_{p-p}^I(\eta, p_{t,h})}{d\eta d^2 p_{t,h}} \\ &= \frac{1}{\sigma_{in}} \int \frac{dz}{z} d^2 p_{t,h} J_1(\eta_g; p_{t,h}; m_{eff}) D(z, p_{t,h}) \delta^2(p_{t,h} - z p_{t,g}) \frac{d\sigma_{p-p}^I(y, p_{t,g})}{dy d^2 p_{t,g}} \Big|_{y \rightarrow \eta_g} \\ &\equiv c(\sqrt{s}) \int d^2 p_{t,g} J_1(\eta; p_{t,g}; m_{eff}) \frac{d\sigma_{p-p}^I(y, p_{t,g})}{dy d^2 p_{t,g}} \Big|_{y \rightarrow \eta}, \end{aligned} \quad (5)$$

where the Jacobian is

$$J_1(\eta; p_t; m_{eff}) = \frac{\cosh \eta}{\sqrt{\frac{m_{eff}^2 + p_t^2}{p_t^2} + \sinh^2 \eta}}, \quad (6)$$

and we neglect the fragmentation function  $D(z, p_{t,h})$ . Corrections to the kinematics due to the hadron mass are considered by replacing  $p_t^2 \rightarrow p_t^2 + m_{eff}^2$  in the evaluation of  $x_{1/2}$ . Assuming pions in  $p - p$  collisions are produced via  $\rho$ -resonance, we take  $m_{eff} = 770 MeV$ .

Component II. According to the quark recombination model [14], the valence quarks of incident proton tend to fly through the central region with their original momentum

fraction. These valence quarks recombine with lower  $p_t$  antiquarks and produce the outgoing hadrons in the fragmentation region. The quark recombination model has explained successfully the meson inclusive distributions and the leading particle effects in the fragmentation region below RHIC energies [18].

The cross section for inclusive pion production in  $p - p$  collisions in the quark recombination model is

$$\begin{aligned} & \frac{1}{\sigma_{in}} \frac{d\sigma_{p-p}^{II}}{dx dp_t^2} \\ &= 6 \frac{1-x}{x} \int_0^x dx_1 x_1 v_p(x_1, p_t^2) \frac{1}{2} (1 + \delta)(x - x_1) s_p(x - x_1, p_t^2), \end{aligned} \quad (7)$$

where  $\delta s_p(x, p_t^2)$  is the distribution of additional sea quarks in the central region and we assume that it has the form like  $s_p(x, p_t^2)$ .

We introduce the rapidity for pions in the recombination processes as

$$y = \ln x - \ln \frac{\sqrt{m_\pi^2 + p_t^2}}{\sqrt{s}}. \quad (8)$$

Thus, we have

$$\frac{1}{\sigma_{in}} \frac{d\sigma_{p-p}^{II}(y, p_t)}{dy dp_t^2} = J_{II}(y; p_t; m_\pi) \frac{1}{\sigma_{in}} \frac{d\sigma_{p-p}^{II}(x, p_t)}{dx dp_t^2} \Big|_{x \rightarrow y}, \quad (9)$$

with a new Jacobian

$$J_{II}(y; p_t; m_\pi) = \frac{\partial x}{\partial y} = \frac{\sqrt{p_t^2 + m_\pi^2}}{\sqrt{s}} e^y, \quad (10)$$

and they lead to



$$\frac{dN_{p-p}^{II}}{d\eta} = \frac{1}{\sigma_{in}} \int dp_t^2 \frac{d\sigma_{p-p}^{II}(\eta, p_t)}{d\eta dp_t^2} = \frac{1}{\sigma_{in}} \int dp_t^2 J_{II}(\eta; p_t; m_\pi) \left. \frac{d\sigma_{p-p}^{II}(y, p_t)}{dy dp_t^2} \right|_{y \rightarrow \eta}, \quad (11)$$

where we integrate over transverse momenta in Eq. (11) at  $p_t < 1\text{GeV}$ , since the recombination model works at lower  $p_t$  range.

Summing the contributions of two components, we have the total distribution

$$\frac{dN_{p-p}}{d\eta} = \frac{dN_{p-p}^I}{d\eta} + \frac{dN_{p-p}^{II}}{d\eta}. \quad (12)$$

The production mechanisms (I) and (II) use unintegrated and integrated parton distributions, respectively. In particular, the gluon momentum fraction in Eqs. (1) and (7) contain both smaller and larger  $x$  regions. Therefore, a set of consistent integrated and unintegrated parton distributions in protons and heavy nuclei, which are defined in a broad kinematic region, are necessary. Fortunately, such parton distributions are proposed in Ref. [8], where the integrated parton distributions are evolved by using a modified DGLAP equation [15] in a whole pre-saturation region; while the unintegrated parton distributions are obtained directly from these integrated parton distributions using the Kimber, Martin and Ryskin (KMR) scheme [19]. We shall use these parton distributions to predict the particle multiplicity distributions.

### 3 Proton-proton collisions

We calculate the pion distributions in  $p-p$  collisions using the two component model and compare the results with the data. We need the values of the total inelastic cross section  $\sigma_{in}$ , which is included by the coefficient  $c(\sqrt{s})$  of Eq. (5). This is rather complicated at the parton level since it contains the nonperturbative information. In this work, we use the midrapidity density for  $p-p(\bar{p})$  collisions to estimate the values of  $c(\sqrt{s})$ . The former has been parameterized by the UA5 [20] and CDF [21] collaborations as

$$\left. \frac{dN_{p-p}}{d\eta} \right|_{\eta=0} = 2.5 - 0.25 \ln s + 0.023 \ln^2 s. \quad (13)$$

This purely empirical parametrization is fitted in a broad range from  $\sqrt{s} = 15\text{GeV}$  to  $1.8\text{TeV}$  and we extend it to the LHC energies. The resulting  $c(\sqrt{s})$  is shown in Fig.1.

Figure 2 shows our results for  $dN_{p-p}/d\eta$  bellow LHC energies with  $m_{eff} = 770\text{MeV}$  (solid curves). The data are taken from Ref.[20]. For comparison, we also draw the distributions with  $m_{eff} = 0$ . We find that the shape of the central rapidity plateau relates sensitively to the value of parameter  $m_{eff}$ . As shown in Fig.2, corresponding to  $m_{eff} = 770\text{MeV}$ , the full rapidity plateau has two peaks. During the reduction of the  $m_{eff}$  value, the rapidity plateau is flattened at  $|\eta| < 2$  and even disappears.

To illustrate the contributions from two production components in our model, in Figs.3 and 4 we use dashed and dotted curves to indicate the contributions from the gluon fusion and quark recombination models, respectively. Although the saturation models [6,7] have used a single gluon fusion mechanism to reproduce these data, they both take a fixed gluon distribution  $\sim (1-x)^4$  at the pre-saturation range. Now we use a reasonable gluon distribution instead of  $(1-x)^4$ . One can find that the resulting dashed curves are narrower

than the solid curves (which are consistent with the data in Fig. 2) in Figs. 3 and 4, and this implies that an additional contribution from the fragmentation regions is necessary.

We predict the pion distributions in  $p - p$  collisions at LHC energies in Figs.5-9. Although the contributions of the quark recombination model (dotted curves) are generally smaller than that of the gluon-gluon fusion model (dashed curves), the contributions of the quark recombination still can not be neglected in the fragmentation region.

Several partonic models have predicted the pion distributions in  $p - p$  collisions at LHC energies. It is interest to compare our results with them. Figure 10 presents the predictions of KLN work [6] (dashed curve) and the comparison with our result (solid curve). Figure 11 compares the comparisons of our prediction with those of the PYTHIA model, which is based on string fragmentation mechanism [22], and PHOJET model, which uses a Pomeron exchange [23]. Figure 12 is a similar comparison with the ultrarelativistic quantum molecular dynamics (UrQMD) model [24]. We think that the comparisons with different models can provide useful knowledge about the unintegrated gluon distribution in the proton and a correct picture of hadron collisions.

## 4 Nucleus-nucleus collisions

The nucleus-nucleus collisions are much more complicated than  $p - p$  collisions. The high multiplicities in heavy-ion collisions typically arise from the large number of nucleon-nucleon collisions. In the analysis of heavy-ion collision data at highly relativistic energies, two parameters which characterize the influence of nuclear geometry are used [25]: (1) the number of participating nucleons  $N_{part}$ , which depends on the collision geometry, and (2) the number of binary nucleon-nucleon collisions  $N_{coll}$ , or the average struck number of each participating nucleon as it passes through the oncoming nucleus,  $\bar{\nu} = N_{coll}/(0.5N_{part})$ . In nuclear collisions, the soft (or hard) component is proportional to the number of participants  $N_{part}$  (or the number of binary collisions  $N_{coll}$ ) [26]. Essentially, we write

$$\frac{2}{\langle N_{part} \rangle} \frac{dN_{A-A}}{d\eta} = \langle \bar{\nu} \rangle c(\sqrt{s}) \int d^2p_t \frac{d\sigma_{A-A}^I(\eta, p_t)}{d\eta dp_t^2} + \frac{1}{\sigma_{in}} \int d^2p_t \frac{d\sigma_{A-A}^{II}(\eta, p_t)}{d\eta dp_t^2}, \quad (14)$$

where  $\langle \dots \rangle$  is an average value in a giving central cut and we only consider 0–6% cut in this work;  $d\sigma_{A-A}$  implies that the parton distributions are the nuclear parton distributions. According to the geometric approach in Ref.[27], we take the mean number of participants  $N_{part} = 339$  in  $Au - Au$  collisions at  $\sqrt{s} = 130$  and 200GeV, and  $N_{part} = 369$  in  $Pb - Pb$  collisions at  $\sqrt{s} = 5.5$ TeV.

The value of  $\bar{\nu}$  contain the knowledge about the interaction between two collided nuclei. Glauber modeling in high-energy nuclear collisions [28] has pointed out that the number of collisions roughly is

$$\langle N_{coll} \rangle \propto \langle N_{part}^{4/3} \rangle \equiv \lambda \langle N_{part}^{4/3} \rangle. \quad (15)$$

On the other hand, the RHIC data [29] present a slow increase of the coefficient  $\lambda$  with energy  $\sqrt{s}$ . Using these data about  $dN_{Au-Au}/d\eta|_{\eta=0}$  at  $\sqrt{s} = 130 - 200\text{GeV}$ , we take a best fitting:  $\lambda = 29 \ln \sqrt{s}$ .

Now we can "predict" the whole distributions in  $Au - Au$  collisions at  $\sqrt{s} = 130$  and  $200\text{GeV}$ . The results are shown in Figs.13 and 14. Where we keep temporarily the value of parameter  $m_{eff} = 770\text{MeV}$ . The dashed and dotted curves are the contributions of the gluon-gluon fusion model and quark recombination model, respectively. There is a small deviation from the data at  $|\eta| > 5$  since the Fermi motion contributions [30] are neglected in our considerations.

Considering the experimental errors, the inconsistency between the theoretical curves and the RHIC data is still visible, and it suggests that some factors failed in our above considerations. In Figs. 15 and 16, we reduce the value of  $m_{eff}$ . A best fit (solid curves) requests the parameters  $m_{eff} = 400\text{MeV}$ . Compared with our previous result of  $m_{eff} = 770\text{MeV}$  for  $p - p$  collisions in Sec. III, we find that the reduction of  $m_{eff}$  at RHIC  $Au - Au$  collisions is possible.

Finally, we calculate the pseudorapidity distributions in  $Pb - Pb$  collisions at  $\sqrt{s} = 5.5\text{TeV}$ . The differences between lead and gold are neglected. Our results are shown by solid curve in Fig.17, where we take  $m_{eff} = 400\text{GeV}$ ; the dashed, and dotted curves correspond to the contributions from gluon-gluon fusion and quark recombination, respectively.

## 5 Discussions

(i) Limiting fragmentation, is it universal or not?

To separate the trivial kinematic broadening of the  $dN/d\eta$  distribution from more interesting dynamics, the collision data at different energies are viewed in the rest frame of one of the colliding target. Such distributions lead to a striking universality of multi-particle production—limiting fragmentation. This hypothesis states that, at high enough collision energy, when effectively viewed in the target rest frame,  $dN/d\eta'$  exhibits longitudinal scaling and becomes independent of energy in a region around  $\eta' \sim 0$ , where  $\eta' = \eta - y_{beam}$ , [ $y_{beam} = \ln(\sqrt{s}/m_N)$ ]. The hypothesis of limiting fragmentation in high energy hadron-hadron collisions was first suggested in Ref. [16]. From a phenomenological view, the projectile hadron, when seen in the frame of the target, is Lorentz-contracted into a very narrow strongly-interacting pancake which passes through the target, assuming that the total hadronic cross sections would become constant at large center-of-mass energy. If this occurred, the excitation and break-up of a hadron would be independent of the center-of-mass energy and distributions in the fragmentation region would approach a limiting curve. We know that the total hadronic cross-sections are not constant at high energies, therefore, limiting fragmentation should fail. However, limiting fragmentation has been observed in a wider region, even extending nearly to midrapidity, and it is referred to as extended longitudinal scaling [25].

From the partonic point of view, longitudinal scaling in hadron collisions relates to Bjorken scaling of the parton distributions and the production dynamics. An interesting question is whether two component models can keep the limiting fragmentation curve. To answer this question, we plot the shifted pseudorapidity distributions in central  $Au - Au$

collisions at  $\sqrt{s} = 130\text{GeV}$  and  $200\text{GeV}$  in Fig.18. The distributions are scaled by  $N_{part}/2$  to remove the effect of the different number of nucleons participating in the collisions. We find longitudinal scaling (energy independence) over more than three units of rapidity, extending nearly to midrapidity and it is consistent with the RHIC data [31]. In Fig. 19, we present the contributions only from the gluon fusion mechanism, where limiting fragmentation still holds at  $\eta' > -1$ .

However, we compare the similar distributions including  $Pb - Pb$  collisions at  $\sqrt{s} = 5.5\text{TeV}$  (dotted curve) in Fig. 20. We find a smaller deviation from the limiting fragmentation limit at  $\eta' < 0$ , although the distributions at  $\eta' > 0$  still keep longitudinal scaling, where it is dominated by the quark recombination mechanism. Figure 21 shows the comparisons of the contributions from the gluon-gluon fusions. The results indicate the deviation from limiting fragmentation originates from the gluon-gluon fusion mechanism.

Back to the  $p - p$  collisions. In Fig.22 we plot our predicted curves in  $p - p$  collisions from  $\sqrt{s} = 130\text{GeV}$  to  $14\text{TeV}$  with  $\eta'$ . We find that a similar deviation from limiting fragmentation exists at  $-2 < \eta' < 0$  if the energies across over a big range between RHIC and LHC.

We noted that a different deviation from limiting fragmentation at the LHC energy is also predicted by using another kind of parton distributions, i.e., the McLerran-Venugopalan distributions in Ref. [32], where the same gluon-gluon fusion mechanism is used. Therefore, investigation of a possible deviation from the limiting curve will provide insight into the evolution equations for high-energy QCD, although the possible larger systematic errors in experiments may hide the deviation.

We try to understand limiting fragmentation and its violation from the partonic pic-

ture. The gluon distributions in Eq.(1) are really irrelevant to the interaction energy  $\sqrt{s}$  in the parton model [17]. A possible relation of Eq. (1) with the interaction energy is that the kinematic ranges of Bjorken variables  $x_{1/2}$  are  $\sqrt{s}$ -dependent. To illustrate that, we draw the kinematic ranges of two multiplying distributions at three different energies using Eq.(2) in Fig. 23. For example, we fix  $p_t = 0.5\text{GeV}$  in Eq.(2) and take  $m_{eff} = 0$ , thus we have  $\eta = y$ . We can find that at  $y = y_{bim}$  (or  $y' = y - y_{bim} = 0$ ), an extremely small  $x_1 = x_{1,small}$  (or  $x_2 = x_{2,small}$ ) always combines with a larger  $x_2 = x_{2,large}$  (or  $x_1,large$ ). Besides,

$$x_{1,large} = x_{2,large} = \frac{p_t}{m_N}, \quad (16)$$

is independent of  $\sqrt{s}$ , and

$$x_{1,small} = x_{2,small} = \frac{p_t m_N}{s}. \quad (17)$$

Thus, we have

$$\begin{aligned} & F_g(x_{1,large}, q_t, p_t) F_g(x_{2,small}, q_t, p_t) \Big|_{y'=0, \sqrt{s}=200\text{GeV}} \\ & \simeq F_g(x_{1,large}, q_t, p_t) F_g(x_{2,small}, q_t, p_t) \Big|_{y'=0, \sqrt{s}=130\text{GeV}}, \end{aligned} \quad (18)$$

since  $x_{2,small}(W = 130\text{GeV}) \simeq x_{2,small}(\sqrt{s} = 200\text{GeV})$ . On the other hand, the difference between the parameters  $c(\sqrt{s})$  at  $\sqrt{s} = 130$  and  $200\text{GeV}$  is small. Consequently, we have limiting fragmentation near  $y' = 0$  in the gluon-gluon fusion processes in Fig. 20.

However, an obvious difference exists near  $y' = 0$  if we compare the results at the RHIC and LHC energies, i.e.,



$$\begin{aligned}
& F_g(x_{1,large}, q_t, p_t) F_g(x_{2,small}, q_t, p_t) \Big|_{y'=0, \sqrt{s}=200GeV} \\
& \neq F_g(x_{1,large}, q_t, p_t) F_g(x_{2,small}, q_t, p_t) \Big|_{y'=0, \sqrt{s}=5.5TeV},
\end{aligned} \tag{19}$$

since  $x_{2,small}(\sqrt{s} = 5.5TeV) \ll x_{2,small}(\sqrt{s} = 200GeV)$ . Although the decreasing  $c(\sqrt{s})$  with increasing  $\sqrt{s}$  almost compensates for the difference in Eq.(19),  $\sigma_{in} \sim \sqrt{s}$  and  $F_g \sim \sqrt{s}$  belong to really different dynamics; therefore, the results in Fig. 21 show a deviation from limiting fragmentation.

It is different from the gluon-gluon fusion mechanism; the quark recombination model naturally satisfies limiting fragmentation. The reason is as follows. For a given  $y' = \ln x + \ln(m_N/\sqrt{m_\pi^2 + p_t^2})$ , the kinematic ranges of Eq. (7) are  $x_1 \in [x, 0]$  and  $x_2 \in [0, x]$ , which are irrelevant to the energy  $\sqrt{s}$ . Therefore, the resulting rapidity distributions have limiting fragmentation, as we have shown in Fig.20.

(ii) The possible deformation of central rapidity plateau.

A general picture of two components of particle production in hadron-hadron collisions predicts two types of ranges for the distributions of final-state particles: except for limiting fragmentation at the fragmentation ranges, particles near midrapidity in the center-of-mass frame were expected to form a rapidity plateau [17]. A narrow plateau appears in our distributions, its height (but not the width) grows with energy. We point out that the structure of the central plateau relates to the value of parameter  $m_{eff}$  rather than the parton distributions: a larger value of  $m_{eff}$  may structure a plateau with double peaks, while it is flattened with decreasing  $m_{eff}$ , and the plateau even disappears when  $m_{eff} \rightarrow 0$ .

Comparing a best fitting  $m_{eff} = 770\text{MeV}$  in  $p-p$  collisions at  $\sqrt{s} = 200\text{GeV}$  (see Fig.

2) with that of  $m_{eff} = 400\text{MeV}$  in  $Au - Au$  collisions at the same energy (see Fig. 16), the reduction of  $m_{eff}$  is possible in ultra relativistic heavy-ion collisions. An interesting question is: whether this is a QGP effect in the RHIC data.

One of the most exciting research areas in RHIC collisions is to find a new matter, i.e., the QGP, in which quarks and gluons are no longer confined to volumes of hadronic dimensions and hadron masses are reduced under the QCD phase transition. One of the conditions in forming the QGP is that a sizable fraction of the initial kinetic energy creates many thousands of particles in a limited volume. Therefore, we consider that the QGP is formed after gluon-gluon collision in the central region in ultrarelativistic heavy-ion collisions. The effective mass  $m_{eff}$  in Eq. (4) will be lowered if part of the minijets go through the QGP region, since that is where chiral symmetry is restored. We regard this decreasing value of  $m_{eff}$  as a QGP effect partly due to the restoration of chiral symmetry. Of course, since large errors occur with the RHIC data in the region  $\eta < 3$  [31], more accurate data are necessary. However, if the above-mentioned QGP corrections to the RHIC data are true, one can expect a more obvious effect in  $Pb - Pb$  collisions at LHC. In Fig.24, we plot such effects in the central plateau of  $Pb - Pb$  collisions at  $\sqrt{s} = 5.5$  TeV where the values  $m_{eff}$  are reduced from 400 MeV to 0.

(iii) How large are the nuclear shadowing effects?

It has been observed [33] that the quark distributions in a nucleus is depleted in the low region of  $x$ , and this is called nuclear shadowing. Our parton distributions [8] include nuclear shadowing corrections through the QCD evolution equations. To illustrate the shadowing effects in the multiplicity productions, we use the following scaled distributions by  $\langle N_{coll} \rangle = \langle 0.5N_{part} \rangle \langle \nu \rangle$  to define the nuclear shadowing factor

$$R = \frac{\frac{1}{\langle N_{coll} \rangle} \frac{dN_{A-A}^I}{d\eta}}{\frac{dN_{p-p}^I}{d\eta}} = \frac{\int d^2p_t \frac{d\sigma_{A-A}^I(\eta, p_t)}{\eta dp_t^2 d}}{\int d^2p_t \frac{d\sigma_{p-p}^I(\eta, p_t)}{d\eta dp_t^2}}. \quad (20)$$

The results in  $Au - Au$  collisions at  $\sqrt{s} = 200\text{GeV}$  (solid curve) and  $\sqrt{s} = 5.5\text{TeV}$  (dashed curve) are presented in Fig.25. The calculations are stopped at larger  $\eta$ , where the quark recombination mechanism and Fermi motion effects [30] become important. The  $\eta$ -dependence of the nuclear shadowing factor  $R$  presents a strong energy-dependence. We find that the shadowing corrections to the initial unintegrated gluon distribution cannot be negligible in any studies of the nuclear effects.

(iv) Two component model or single component model?

The early two component picture of hadron-hadron collisions assumes that a broad boost-invariant central plateau is separated by two energy-independent fragmentation regions [17]. However, the following experiments indicate that limiting fragmentation can be extended to beyond fragmentation ranges, and no evidence shows a boost-invariant central plateau [25]. It seems that a single-component mechanism dominates the hadron production. The KLN [6] and Albacete [7] are such single-component models. However, the dashed curves in Figs. 3 and 4, which are determined by the evolved unintegrated gluon distributions, are lower than the data, and it shows that the contributions from two components of production are necessary.

(v) Saturation, it comes or not?

Saturation is a limiting form of the shadowing modified gluon distribution. In this work, we do not consider the corrections of saturation, although shadowing is included. We compare our predictions with those of two saturation models. Kharzeeva, Levin, and Nardi [6] use a single production mechanism [i.e., the component I in Eqs. (12) and (14)]

to predict the heavy-ion collisions at LHC. Instead of the two scale unintegrated gluon distribution in Eq. (1), KLN use a saturated integrated gluon distribution

$$xG(x, p_t^2) = \begin{cases} \frac{\kappa}{\alpha_s(Q_s^2)} S p_t^2 (1-x)^4 & p_t < Q_s(x) \\ \frac{\kappa}{\alpha_s(Q_s^2)} S Q_s^2(x) (1-x)^4 & p_t > Q_s(x) \end{cases}, \quad (21)$$

to calculate the rapidity distributions.  $S$  is the inelastic cross section for the minimum bias multiplicity and  $\kappa$  is a normalization coefficient. A free parameter is  $dN/d\eta|_{\eta=0}$ , which contains nonperturbative information. In the KLN model, it is fixed by the value of  $dN_{Au-Au}/d\eta|_{\eta=0}$  at  $\sqrt{s} = 130$  GeV and assumption

$$\langle \bar{v}(\sqrt{s}) \rangle = c(\sqrt{s}) = const. \quad (22)$$

Figure 26 compares our results in Fig. 17 with the KLN predictions [6].

Albacete [7] uses the same single production mechanism but with a different gluon distribution, which is the solution of the BK equation in the form of single scale distribution.

Albacete assumes

$$\langle N_{part}(\sqrt{s}) \rangle = \langle \bar{v}(\sqrt{s}) \rangle = c(\sqrt{s}) = const., \quad (23)$$

and uses the value  $dN_{Au-Au}/d\eta|_{\eta=0}$  at  $\sqrt{s} = 200$  GeV to fix this constant. Figure 27 compares our results with the Albacete predictions [7].

Except for the contributions of quark recombination and different values of  $m_{eff}$ , the differences among three models originate from the different parton distributions, which obey different QCD evolution dynamics. Therefore, the observations of the multiplicity distributions are useful in identifying a true QCD evolution dynamics in the upcoming LHC data.

(vi) Validity of the factorization formula Eq. (1). We noted that the works in Ref. [34] presented a covariant gauge calculation, where the transverse momentum spectrum of the gluon is perturbatively determined by the final-state interactions of the gluon with the nucleons in the nucleus. In this case, the applications of the  $k_t$  factorization formula (1) is unsatisfied. However, these works neglect the QCD evolution of gluons. Our aim is to test the predictions of the MD-DGLAP evolution equation in the LHC physics, where a physical gauge is used for the factorization of the evolution kernel. The above-mentioned final-state interactions are absent, and these effects are absorbed into the phenomenological fragmentation functions. Therefore, the application of Eq. (1) is reasonable in this work.

## 6 Summary

We use two complementary production mechanisms: hard gluon-gluon fusion in the central rapidity region and soft quark recombination in the fragmentation region to study the particle multiplicity distributions in hadron-hadron collisions at high energies. We emphasize that a set of consistent integrated and unintegrated parton distributions, which are well defined in a broad kinematic range are necessary in such partonic model. For this reason, our parton distributions proposed in Ref.[8] are used. Based on the explanations of the present data, we predict the pseudorapidity densities of charged particles produced in  $p - p$  and central  $Pb - Pb$  collisions at LHC energies. We find that the limiting fragmentation hypothesis, which generally appears in the present data of hadron collisions is partly violated if the observations are across a wide range between the RHIC and LHC energies. An explanation about limiting fragmentation and its violation in partonic picture are given. We proposed that a possible QGP effect may deform the shape of the central plateau. In this work, we use an entirely phenomenological parametrization of existing data to fix the energy dependence of normalization factors of the hadronic distributions. This simple method may need modification after we obtain the LHC data at midrapidity. However, once this normalization is fixed, whole particle multiplicity distributions are completely determined by our parton distributions. The comparisons between our model and other partonic models are given. The differences in the predicted distributions in various models can help us to identify the true QCD dynamics in hadron collisions.

**Acknowledgments:** This work was supported by the National Natural Science Foundations of China 10875044.

## References

- [1] For a review, see Small  $x$  Collaboration, B. Andersson et al., Eur.Phys.J. **C25**, 77 (2002), and references therein.
- [2] J.Jalilian-Marian, A. Kovner, L. McLerran and H. Weigert, Phys. Rev. **D55**, 5414, (1997); J.Jalilian-Marian, A. Kovner, A. Leonidov and H. Weigert, Nucl. Phys. **B504**, 415 (1997); H. Weigert, arXiv:hep-ph/0004044; E. Iancu, A. Leonidiv and L. McLerran, Nucl. Phys. **A692**, 583 (2001).
- [3] K. Rummukainen and H. Weigert, Nucl. Phys. **A739**, 183 (2004).
- [4] I. Balitsky, Nucl. Phys. **B463**, 99 (1996); Y. V. Kovchegov, Phys. Rev. **D60**, 034006 (1999).
- [5] D. Kharzeev and E. Levin, Phys. Lett. **B523**, 79 (2001).
- [6] D. Kharzeeva, E. Levin and M. Nardi, Nucl. Phys. **A747**, 609 (2005).
- [7] J.L. Albacete, Phys. Rev. Lett. **99**, 262301 (2007).
- [8] J.H. Ruan and W. Zhu Phys. Rev. **C80**, 045209 (2009).
- [9] A. Szczurek, Acta Phys. Polon. **B34**, 3191 (2003).
- [10] L.V. Gribov, E.M. Levin and M.G. Ryskin, Phys. Rep. **100**, 1 (1983).
- [11] S. Pokorski and L. Van Hove, Acta Phys. Pol. **B5**, 229 (1974); W. Ochs, Nucl. Phys. **B118**, 397 (1977).

- [12] X.N. Wang and M. Gyulassy, Phys. Rev. **D44**, 3501 (1991); X.N. Wang, Phys. Rept. **280**, 287 (1997).
- [13] B. Andersson, G. Gustafson, B. Nilsson-Almqvist, Nucl. Phys. **B281**, 289(1987); B. Nilsson-Almqvist, E. Stenlund, Comput. Phys. Commun. **43**, 387 (1987).
- [14] K.P. Das and R.C. Hwa, Phys. Lett. **68B**, 459 (1977); R.C. Hwa, Phys. Rev. **D22**, 1593 (1980).
- [15] W. Zhu, Nucl. Phys. **B551**, 245 (1999); W. Zhu and J.H. Ruan, Nucl. Phys. **B559**, 378 (1999); W. Zhu and Z.Q. Shen, HEP & NP, **29**, 109 (2005).
- [16] J. Benecke, T.T. Chou, C.N. Yang and E. Yen, Phys. Rev. **188**, 2159 (1969). T.T. Chou and C.N. Yang, Phys. Rev. Lett. **25**, 1072 (1970).
- [17] R. P. Feynman, Phys. Rev. Lett. **23**, 1415 (1969).
- [18] R.G. Roberts. P.C. Hwa and S. Matsuda, J. Phys. **G5**, 1043 (1979); T.A. DeGrand, Phys. Rev. **D19**, 1398 (1979).
- [19] M. A. Kimber, A. D. Martin and M. G. Ryskin, Phys. Rev. **D63**, 114027 (2001); M. A. Kimber, A. D. Martin and M. G. Ryskin, Eur. Phys. J. **C12**, 655 (2000).
- [20] G.J. Alner, et al., (UA5 Colaboration), Zeit. Phys. **C33**, 1 (1986); G.J. Alner, et al., (UA5 Colaboration), Phys. Lett. **167B**, 476 (1986).
- [21] F. Abe, et al., (CDF Collaboration), Phys. Rev. Lett. **61**, 1819 (1989).



- [22] T. Sjostrand, et al., Computer Physics Commun. **135**, 238 (2001); T. Sjostrand and M. van Zijl, Phys. Rev. **D36**, 2019 (1987); T. Sjostrand and P. Skands, Eur. Phys. J. **C39**, 129 (2005).
- [23] R. Engel, Z. Phys. **C66**, 203 (1995); R. Engel, J. Ranft and S. Roesler, Phys. Rev. **D52**, 1459 (1995).
- [24] M. Mitrovski, T. Schuster G. Graef, H Petersen and M. Bleicher, Phys. Rev. **C79**, 044901 (2009).
- [25] B.B.Back et. al., (PHOBOS Collaboration), Nucl.Phys. **A757**, 28 (2005).
- [26] X.-N. Wang and M. Gyulassy, Phys. Rev. Lett. **86**, 3496 (2001).
- [27] D. Kharzeev, M. Nardi, Phys.Lett. **B507**, 121 (2001).
- [28] M.L. Miller, K. Reygers, S.J. Sanders and P.Steinberg, Ann. Rev. Nucl. Part. Sci. **57**, 205 (2007).
- [29] B. B. Back et al., (PHOBOS Collaboration), Phys. Rev. Lett. **87**, 102302 (2001); B. B. Back et al., (PHOBOS Collaboration), Nucl. Phys. **A698**, 416c (2002).
- [30] C.H. Lewellyn Smith, Phys. Lett. **128B**, 107 (1983).
- [31] B. B. Back et al., (PHOBOS Collaboration), Phys.Rev.Lett. **91**, 052303 (2003).
- [32] F. Gelis, A.M. Stasto and R. Venugopalan. Eur. Phys. J. **C48**, 489 (2006).
- [33] EM Collab., J. Ashman, et al., Phys. Lett. **202B**, 603 (1988); EM Collab., M. Arneodo, et al., Phys. Lett. **211B**, 493 (1988).

- [34] Y. V. Kovchegov and A.H. Mueller, Nucl. Phys. **B529**, 451 (1998); Y. V. Kovchegov and K Tuchin, Phys. Rev. **D65**, 074026 (2002).

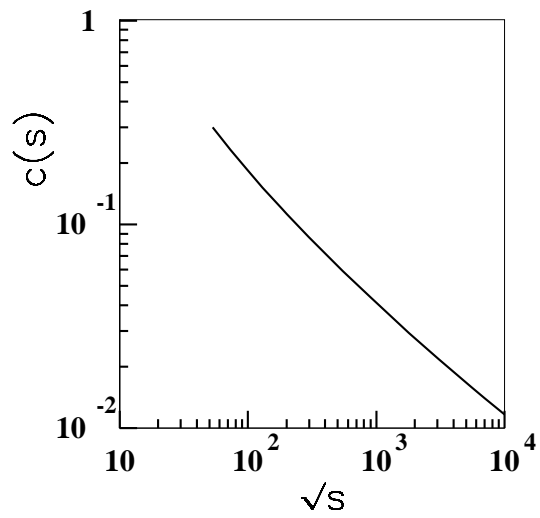


Fig. 1 Coefficient  $c(\sqrt{s})$  in Eq.(5) plotted as a function of energy  $\sqrt{s}$  using Eq.(13).

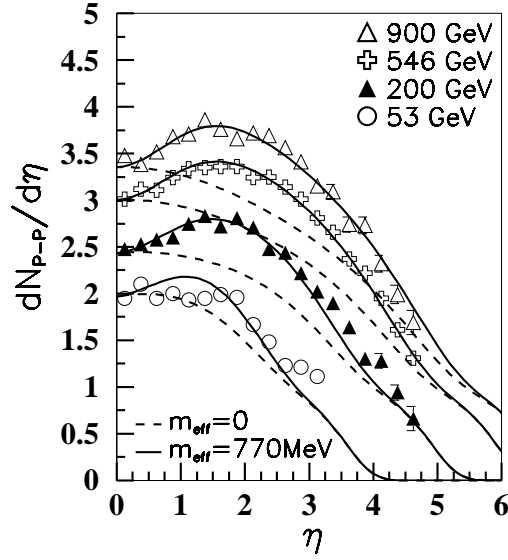


Fig. 2 Computed pseudo-rapidity distribution of charged particles in  $p - p(\bar{p})$  collisions at various energies with  $m_{eff} = 770\text{MeV}$  and  $\delta = 0.7$  (solid curves). The dashed curves take  $m_{eff} = 0$ . The data are taken from Ref. [20].

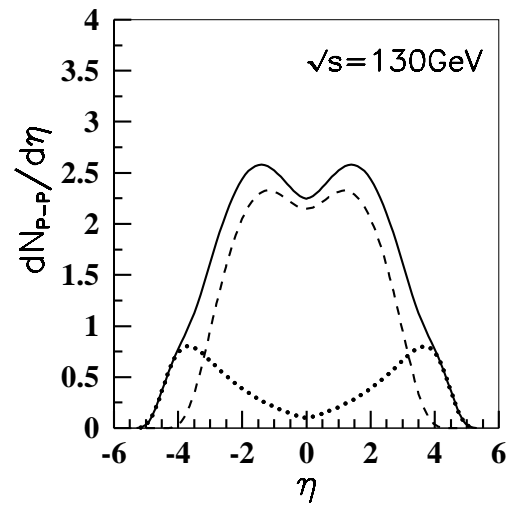


Fig. 3 Solid curve in Fig.2 at  $\sqrt{s} = 130\text{GeV}$ , where dashed and dotted curves are the contributions of gluon fusion mechanism I and quark recombination mechanism II.

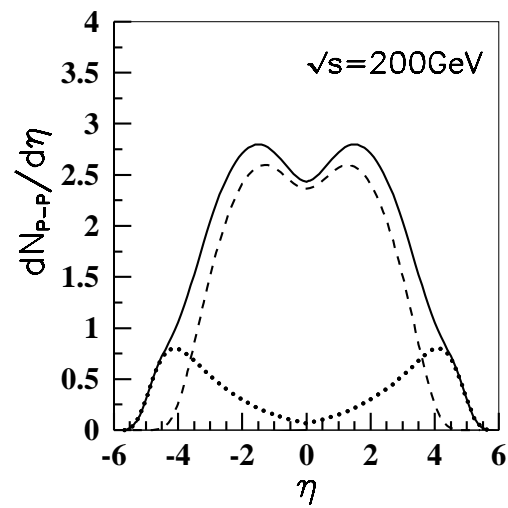


Fig. 4 Similar to Fig.3 but at  $\sqrt{s} = 200 \text{ GeV}$ .

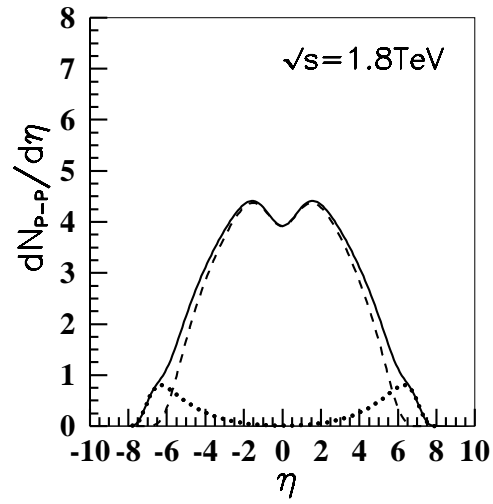


Fig. 5 Predicted pseudorapidity distribution of charged particles in  $p - p$  collisions at  $\sqrt{s} = 1.8\text{TeV}$ . Dashed and dotted curves are the contributions of the gluon fusion model (I) and quark recombination model (II).

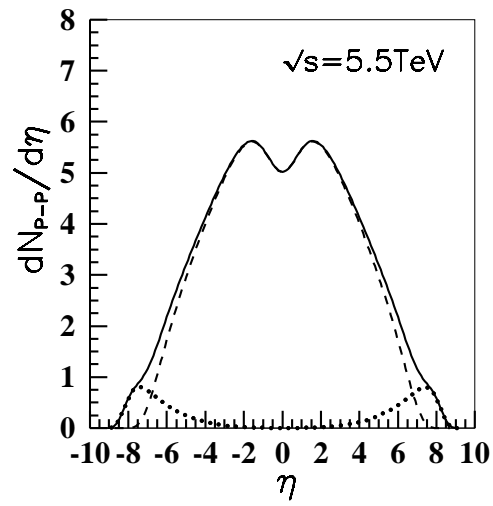


Fig. 6 Similar to Fig. 5 but at  $\sqrt{s} = 5.5\text{TeV}$ .



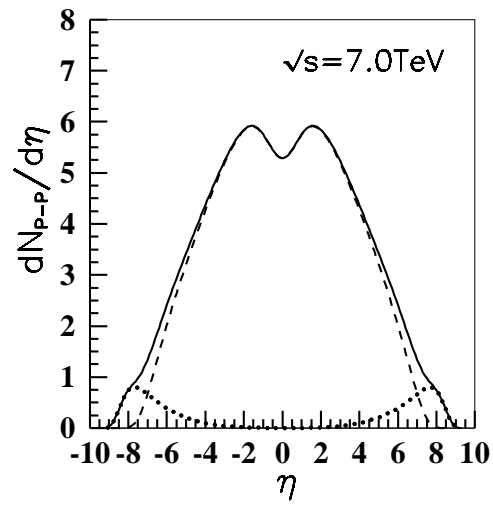


Fig. 7 Similar to Fig. 5 but at  $\sqrt{s} = 7 \text{ TeV}$ .

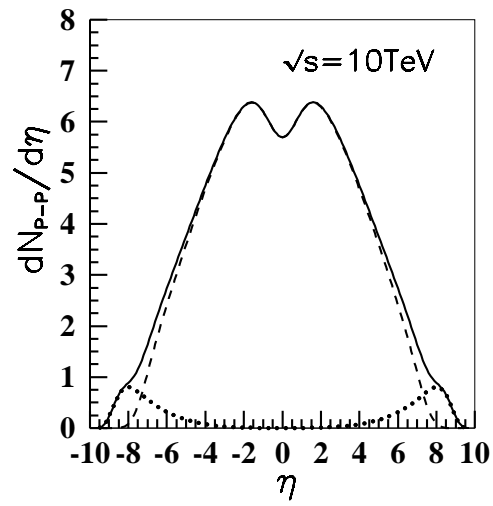


Fig. 8 Similar to Fig. 5 but at  $\sqrt{s} = 10 \text{ TeV}$ .

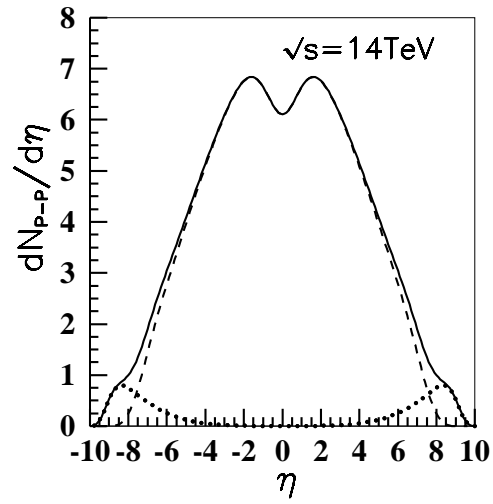


Fig. 9 Similar to Fig. 5 but at  $\sqrt{s} = 14 \text{ TeV}$ .

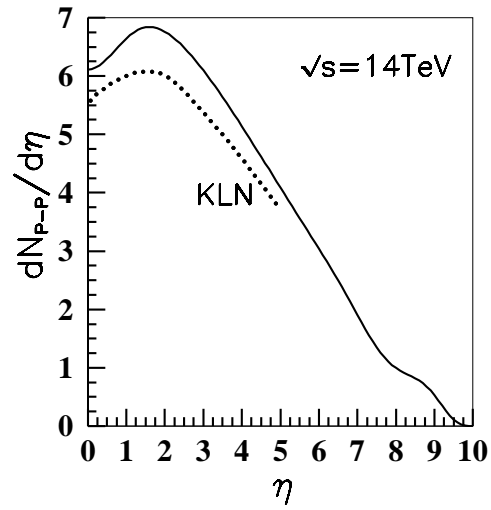


Fig. 10 Comparisons of our predictions (solid curve) for pseudorapidity distribution of charged particles in  $p-p$  collisions at  $\sqrt{s} = 14\text{TeV}$  with that of KLN predictions (dashed curve) [6].

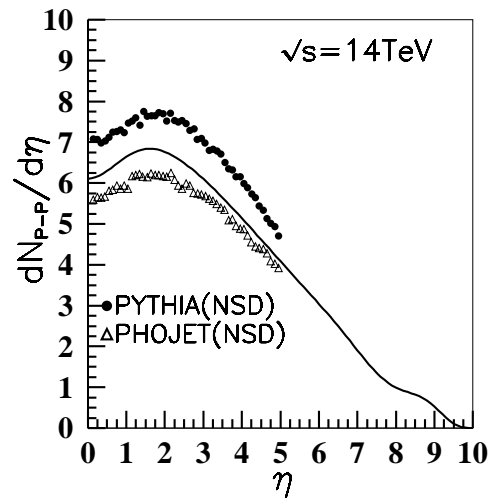


Fig. 11 Comparisons of our predictions (solid curve) for pseudo-rapidity distribution of charged particles in  $p - p$  collisions at  $\sqrt{s} = 14 \text{ TeV}$  with that of PYTHIA [22] and PHOJET models [23].

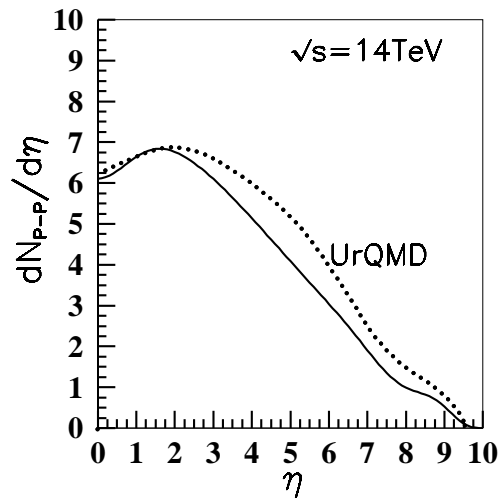


Fig. 12 Comparisons of our predictions (solid curve) for pseudorapidity distribution of charged particles in  $p - p$  collisions at  $\sqrt{s} = 14\text{TeV}$  with that of the UrQMD model (dashed curve) [24].

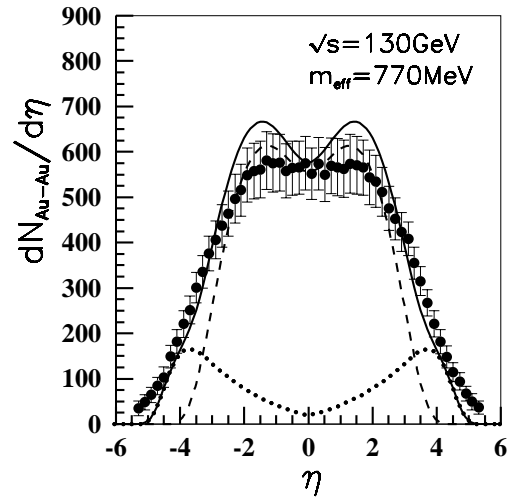


Fig. 13 Pseudo-rapidity density of charged particles produced in  $Au - Au$  collisions with 0–6% central cut at  $\sqrt{s} = 130$  GeV. Data are taken from [29]. The solid curve corresponds to  $m_{\text{eff}} = 770 \text{ MeV}$ . Dashed and dotted curves are the contributions of the gluon-gluon fusion and quark recombination, respectively.

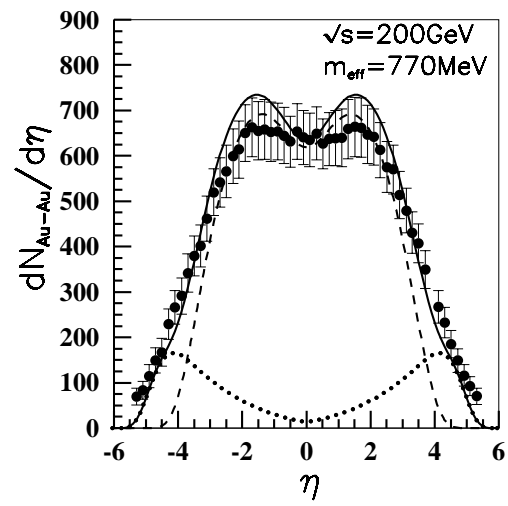


Fig. 14 Same as Fig.13 but for  $\sqrt{s} = 200\text{GeV}$ .



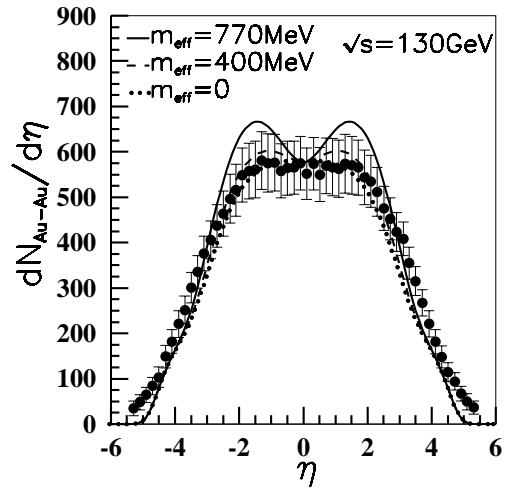


Fig. 15 Pseudorapidity density of charged particles produced in  $Au - Au$  collisions with 0 – 6% central cut at  $\sqrt{s} = 130 GeV$  with different parameters  $m_{eff} = 770 MeV$  (solid curve), 400MeV (dashed curve), and 0 (dotted curve). Data with errors are taken from [29].

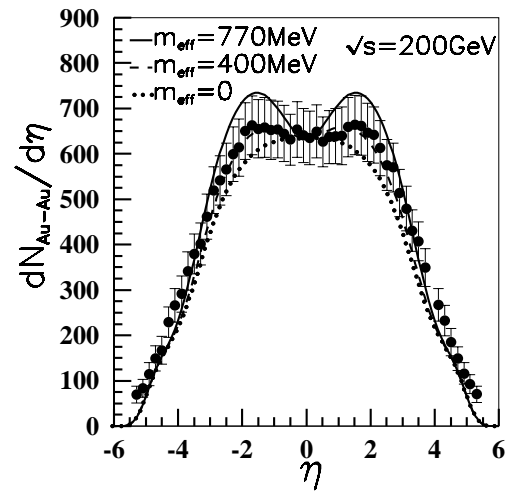


Fig. 16 Same as Fig.15 but at  $\sqrt{s} = 200$  GeV.

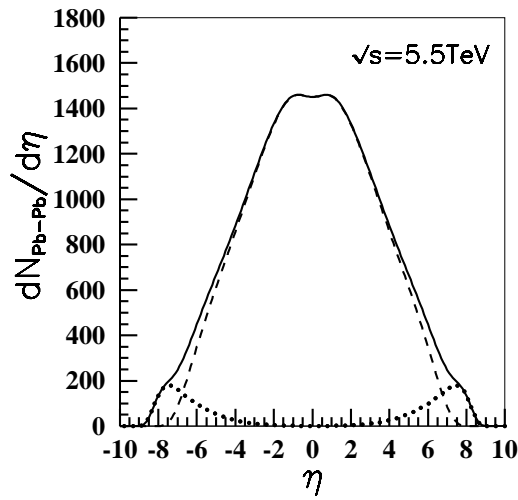


Fig. 17 Predictions of pseudo-rapidity density of charged particles produced in  $Pb - Pb$  collisions with 0 – 6% central cut at  $\sqrt{s} = 5.5$  TeV. Dashed and dotted curves are the contributions of the gluon-gluon fusion and quark recombination, respectively

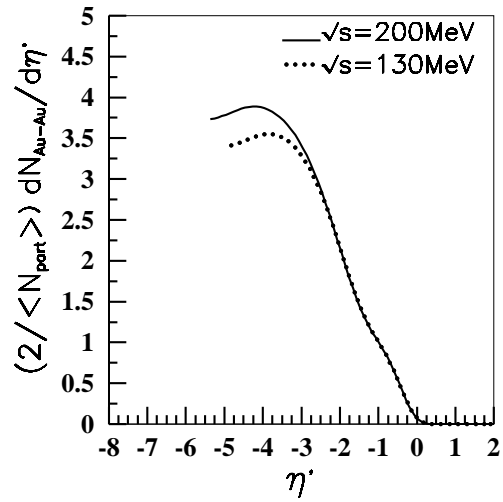


Fig. 18 Shifted and scaled pseudorapidity distribution of charged particles produced in  $Au - Au$  collisions with 0 – 6% central cut at  $\sqrt{s} = 130 \text{ GeV}$  (dashed curve) and  $200 \text{ GeV}$  (solid curve). Results exhibit limiting fragmentation at  $\eta' > -1.5$ .

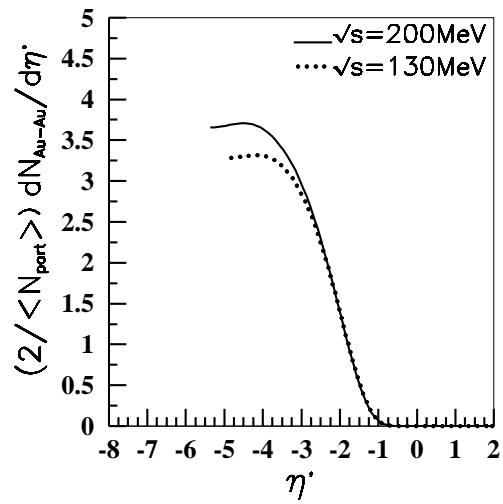


Fig. 19 Similar to Fig.18 but with contributions from gluon-gluon fusion mechanism. The same limiting fragmentation appears.

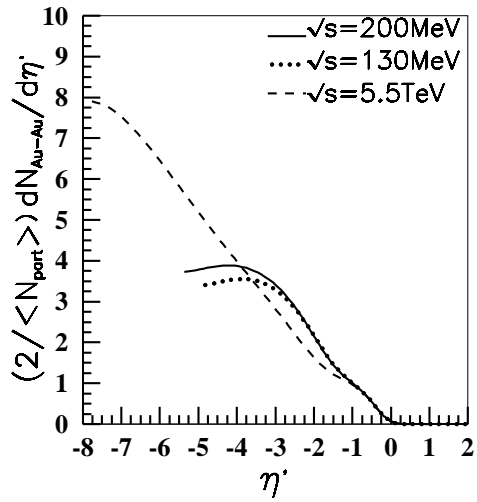


Fig. 20 Comparisons of shifted and scaled pseudorapidity distribution of charged particles produced in  $Pb - Pb$  collisions with 0 – 6% central cut at  $\sqrt{s} = 5.5\text{TeV}$  (dotted curve) with the curves of Fig. 18. Results exhibit deviations from limiting fragmentation at  $\eta' < 0$

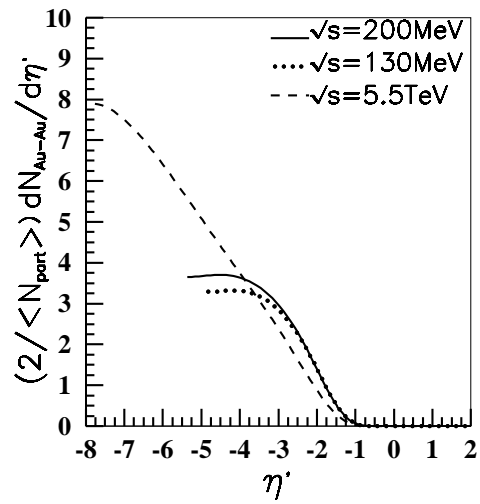


Fig. 21 Similar to Fig.20 but with contributions from the gluon-gluon fusion mechanism.

Similar violations of limiting fragmentation appear.

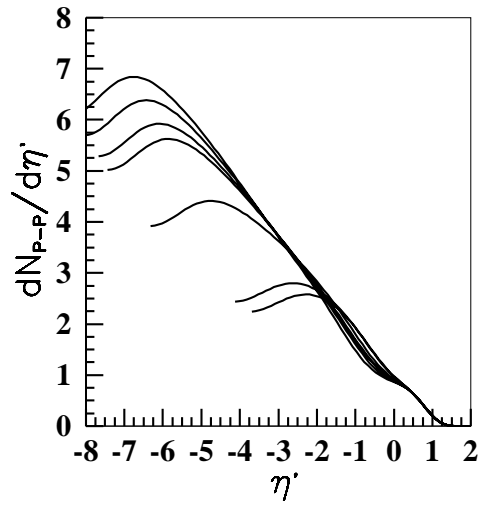


Fig. 22 Predicted  $dN_{N-N}/d\eta'$  at 0–6% central vs the shifted pseudo-rapidity  $\eta' = \eta - y_{beam}$  in a range of energies corresponding to Figs.3-9 ( $\sqrt{s} = 130\text{GeV}-14\text{TeV}$  from bottom to top). The results exhibit longitudinal scaling and a small violation as in Fig. 21.



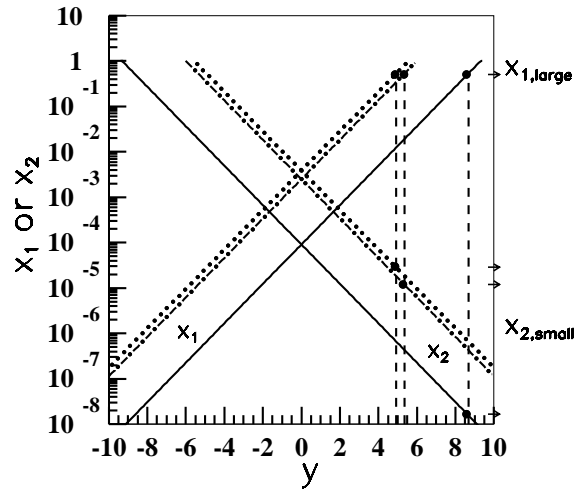


Fig. 23 Kinematical ranges of  $x_{1/2}$  with different energies  $\sqrt{s}$  and  $p_t = 0.5\text{GeV}$  in Eq.(2): Solid curves:  $\sqrt{s} = 5.5\text{TeV}$ ; Dashed-dotted curves:  $\sqrt{s} = 200\text{GeV}$  and dotted curves:  $\sqrt{s} = 130\text{GeV}$ . Vertical dashed curves correspond to (from left to right)  $y' = 0$  at  $\sqrt{s} = 130\text{GeV}$ ,  $200\text{GeV}$  and  $5.5\text{GeV}$ .

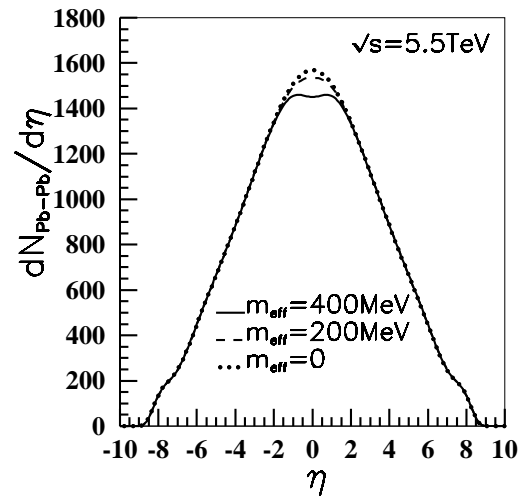


Fig. 24 Deformation of central rapidity plateau with decreasing parameter  $m_{eff}$  in  $Pb-Pb$  collisions at  $\sqrt{s} = 5.5$  TeV. Solid, dashed, and dotted curves correspond to  $m_{eff} = 400\text{MeV}$ ,  $200\text{MeV}$  and  $0$ .

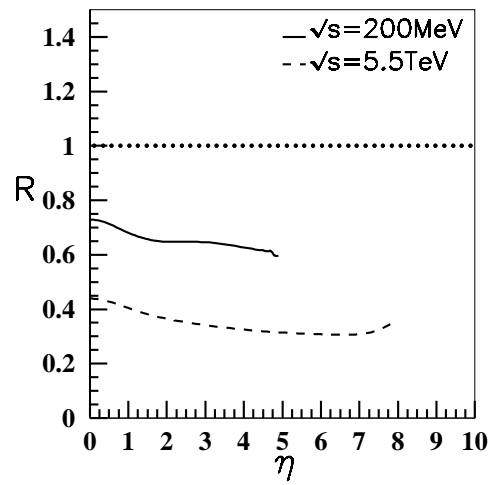


Fig. 25 Nuclear shadowing factor  $R$  in Eq.(20) at different energies  $\sqrt{s}$ , where the pseudorapidity distributions in  $Au - Au$  collisions are scaled by  $N_{coll}$ .

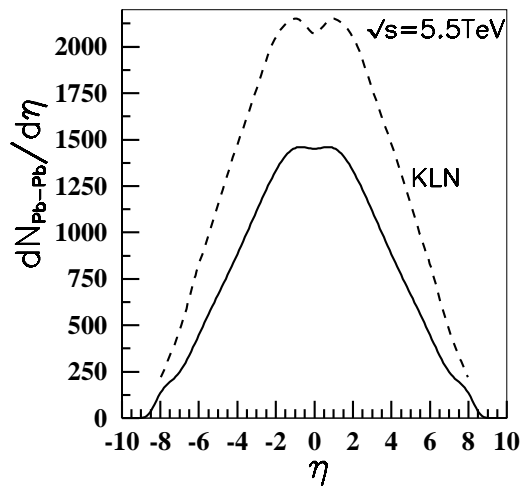


Fig. 26 Comparison of our predictions in Fig.17 with the results of the KLN model [6] (dotted curve), where  $m_{eff} = 500$  MeV in the KLN model.

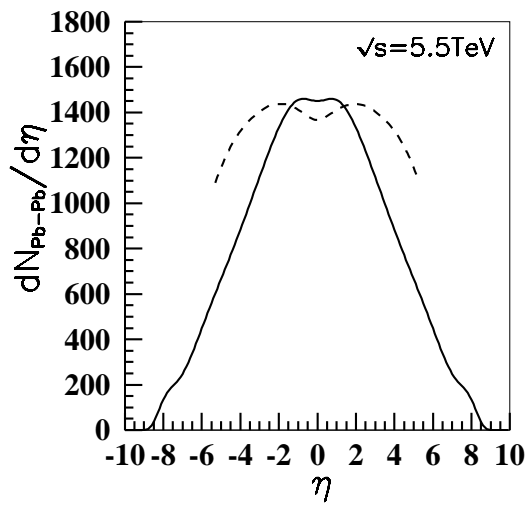


Fig. 27 Comparison of our predictions in Fig.17 with the results of the Albacete model [7] (dotted curve), where  $m_{eff} = 250\text{MeV}$  in the Albacete model.